# Characteristics of surface sound pressure and absorption of a finite impedance strip for a grazing incident plane wave

K. S. Sum[a] and J. Pan[b]
*School of Mechanical Engineering, The University of Western Australia, 35 Stirling Highway, Crawley, Western Australia 6009, Australia*

(Received 22 August 2006; revised 4 February 2007; accepted 10 February 2007)

Distributions of sound pressure and intensity on the surface of a flat impedance strip flush-mounted on a rigid baffle are studied for a grazing incident plane wave. The distributions are obtained by superimposing the unperturbed wave (the specularly reflected wave as if the strip is rigid plus the incident wave) with the radiated wave from the surface vibration of the strip excited by the unperturbed pressure. The radiated pressure interferes with the unperturbed pressure and distorts the propagating plane wave. When the plane wave propagates in the baffle-strip-baffle direction, it encounters discontinuities in acoustical impedance at the baffle-strip and strip-baffle interfaces. The radiated pressure is highest around the baffle-strip interface, but decreases toward the strip-baffle interface where the plane wave distortion reduces accordingly. As the unperturbed and radiated waves have different magnitudes and superimpose out of phase, the surface pressure and intensity increase across the strip in the plane wave propagation direction. Therefore, the surface absorption of the strip is nonzero and nonuniform. This paper provides an understanding of the surface pressure and intensity behaviors of a finite impedance strip for a grazing incident plane wave, and of how the distributed intensity determines the sound absorption coefficient of the strip. © *2007 Acoustical Society of America.* [DOI: 10.1121/1.2713710]

PACS number(s): 43.55.Ev, 43.55.Dt, 43.20.El [NX] Pages: 333–344

## I. INTRODUCTION

The relationship between the plane wave reflection coefficient, $R_L$, and the specific normal acoustical impedance, $\zeta_L$, of an infinitely flat boundary of local reaction (also known as an impedance boundary) is well known and given by

$$R_L = \frac{\zeta_L \cos\theta - 1}{\zeta_L \cos\theta + 1}, \tag{1}$$

where $\theta$ is the incident angle of the plane wave relative to the normal of the boundary. Equation (1) relates the impedance to the sound absorption coefficient of the boundary for plane wave excitations at oblique incidence and diffuse incidence.[1–3] It also allows the impedance to be related to the decay rates of acoustic modes[4,5] and diffuse sound fields in rooms.[1,6] In addition, the equation has been extensively used in the development of many experimental techniques for measuring surface impedances of porous and nonporous materials.[7–9] It is also a basis for the image method[10] in architectural acoustics, and numerous studies of sound fields above boundaries of local or extended reaction in outdoor sound propagation.[11–14]

However, at $\theta=90°$ when the plane wave grazes the impedance boundary, Eq. (1) becomes problematic for any nonzero value of $\zeta_L$. In this case, $R_L=-1$ where the incident and reflected waves have an equal magnitude but are 180° out of phase when they completely cancel each other. Therefore, there is no sound pressure above the boundary and this is practically not possible. Also, the sound absorption coefficient of the boundary ($=1-|R_L|^2$) is zero, which implies that the boundary does not absorb sound at all. This condition can still exist even though monopole or dipole sources are used if the emitted spherical waves are decomposed into plane wave components.[8] It can also be present in the absorption of periodically arranged absorptive materials as long as Eq. (1) is invoked.[15] Traditionally, workers have avoided the problem with grazing plane waves by using a point source and considering the incident wave to be spherical, where the sound field above the boundary is described in terms of the Sommerfeld integrals as well as an integral with a Bessel function of zero order.[11–14,16,17] Although these integrals do not lead to a zero pressure for a grazing incident wave, many relevant past studies were mainly mathematical, and much effort was focused on investigating the characteristics of the integral with the Bessel function and the pole of this integral.[13,16,17] In addition, this integral is too complicated for an exact analytical solution of the sound pressure to be obtained so asymptotic analytical solutions have been proposed for any incident angle of the spherical wave. But, most reported works that employed these solutions only dealt with either the application/development of methods for predicting the sound pressure above the boundary,[11,12,14] or the formulation and validation of techniques for predicting the impedance and absorption coefficient of the boundary.[18–22]

In rooms, boundaries are finite and acoustical mode shapes can be observed when the sound fields are not diffuse. For rectangular rooms, it is known that these modes are identifiable and composed of propagating plane waves in regions which are sufficiently far from the sound source, even when the source emits spherical waves. Thus, the planar nature of

[a]Electronic mail: ksum@mech.uwa.edu.au
[b]Electronic mail: pan@mech.uwa.edu.au

the incident wave that impinges upon a boundary cannot be simply neglected. However, based on experimental observations that absorption coefficients of impedance surfaces in rectangular rooms are nonzero (the surfaces absorb sound) for grazing plane waves,[23] reflected wave fronts were believed to have curvatures when incident angles of plane waves are far from the normals of the surfaces. From a recent study, one may also expect these curvatures to be significant for highly absorptive surfaces and at very low frequencies as under such conditions, the sound pressures in rectangular rooms could not be accurately predicted using the plane wave reflection coefficient [i.e., Eq. (1)].[24] These past works focused on the measurement of surface absorption coefficients at resonances of rooms[23] and accuracy of predictive models for room acoustics.[24] Also, many published studies on absorptions of impedance surfaces in rooms only either reported experimental data of absorption coefficients to compare the size/edge effects of the surfaces,[25–27] or applied/developed methods for comparing these effects at normal, oblique, and random incidences of plane waves.[28–32] As a result, the physical picture of the reflected wave front curvature of an impedance boundary and its effect on the boundary absorption is still obscure. It follows that the reason for the curvature, its relationship to the boundary impedance, and the resulting boundary absorption are not clearly understood. Therefore, it is necessary to investigate how both the finiteness and impedance of the boundary determine the shape of the reflected wave front even though the incident wave is planar, and the way that the boundary absorption is related to the behavior of the reflected wave.

In this paper, characteristics of sound pressure and intensity on the surface of a flat and finite impedance strip flush-mounted on a rigid baffle are studied. The specific case of plane wave excitation at grazing incidence is considered. Previous studies for grazing incident plane waves have been concerned only with mathematical analyses of scattering due to rough surfaces.[33,34] The boundary integral method is used, where the surface pressure of the strip is expressed in terms of the superposition between the unperturbed wave and the radiated wave. This method is well established, and has been extensively validated and used for the prediction of pressures above impedance surfaces for spherical[35–37] and plane[3,28,32,38] wave excitations. The unperturbed wave consists of the specularly reflected wave as if the strip is rigid and the incident wave, while the radiated wave arises from the surface vibration of the strip excited by the unperturbed pressure. The total of the reflected and radiated waves is the scattered wave, while the total of the unperturbed and radiated waves is called the perturbed wave. Hence, the "surface pressure" and "surface intensity" terms refer to the perturbed pressure and intensity on the surfaces of both the baffle and the strip, unless one of the surfaces is otherwise specified. A numerical procedure called the quadrature technique[35,36,39] is employed to solve the boundary integral problem. As the present work is concerned with surface acoustical properties, singularities exist in the numerical solutions of surface pressure of the strip. Thus, the quadrature technique is modified to deal with the ill condition and the convergence of the solutions is examined. Examples are used to show the variation of radiated pressure on the surface of the strip with the impedance of the strip as well as with the excitation frequency. The distortion of the propagating plane wave along the strip by this pressure is then illustrated. Characteristics of the resulting surface pressure and intensity across the strip, and the sound absorption coefficient of the strip determined by the intensity distribution, are also studied. This paper provides a visualization of the way that the radiated pressure of a finite impedance strip distorts a plane wave that grazes the strip. It also provides an understanding of the radiated wave effects on the surface pressure and intensity of the strip, how the distributed intensity determines the absorption coefficient of the strip, and the reason why the absorption of the strip is not zero even though the incident wave is a grazing plane wave.

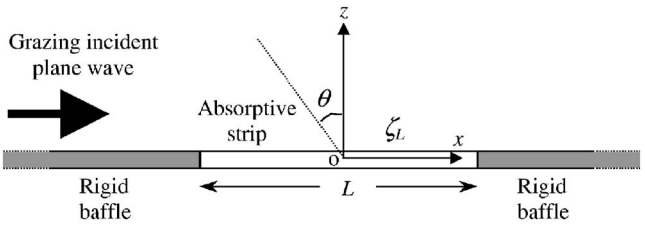


FIG. 1. Schematic illustration of the impedance strip flush-mounted on a rigid baffle and the grazing incident plane wave.

## II. SURFACE PRESSURE AND INTENSITY OF THE STRIP

### A. Formulation of the boundary integral problem

Figure 1 depicts an impedance strip which is flush-mounted on a rigid baffle. $L$ and $\zeta_L$ are the length and the specific acoustical impedance of the strip. The coordinate system is also shown and its origin is located at the center of the strip. First, consider the steady-state excitation by a plane wave at an oblique incident angle of $\theta$ from the normal of the strip. By using the Green's function technique in the two-dimensional acoustic wave equation for the sound field on and above the baffle and the strip, the sound pressure, $p$, at any position $(x,z)$ for $-\infty < x < \infty$ and $z \geqslant 0$, can be derived as[3,28,32,38]

$$p(x,z) = p_{\text{unpt}}(x,z) + p_{\text{rad}}(x,z), \tag{2a}$$

$$p_{\text{unpt}}(x,z) = 2P_{\text{inc}} e^{j\omega t - jkx \sin\theta} \cos(kz\cos\theta), \tag{2b}$$

$$p_{\text{rad}}(x,z) = \int_L G(x,z|x^{(s)},0) \left.\frac{\partial p}{\partial z}\right|_{z=0} dx^{(s)}. \tag{2c}$$

In Eq. (2b), $P_{\text{inc}}$ is the complex pressure amplitude of the plane wave, $t$ is time, $\omega$ is the radian frequency ($=2\pi f$; $f$ is the frequency in hertz), and $k$ is the wave number ($=\omega/c_0$; $c_0$ is the speed of sound in air). In Eq. (2c), $G$ is the Green's function of the sound field for the plane wave excitation, and $x^{(s)}$ is the $x$ coordinate of a point on the surface of the strip (i.e., $z=0$). As the strip is of local reaction, the boundary condition of the sound field on the surface of the strip is

$$\left.\frac{\partial p}{\partial z}\right|_{z=0} = j\rho_0\omega v(x^{(s)}) = \frac{jkp(x^{(s)},0)}{\zeta_L}, \tag{3}$$

where $\rho_0$ is air density, and $v$ is the normal velocity of the surface [note: $v(x^{(s)})=p(x^{(s)},0)/\rho_0 c_0\zeta_L$]. $p_{\text{unpt}}$ given by Eq. (2b) is the unperturbed pressure that consists of the combination of the specularly reflected pressure as if the strip is rigid and the incident pressure. On the surface of the strip, the unperturbed pressure is also widely known as the blocked pressure. $p_{\text{rad}}$ given by Eq. (2c) depends on $\partial p/\partial z|_{z=0}$ that is a function of $v$ [see Eq. (3)] and therefore, it represents the radiated pressure due to the surface vibration of the strip that is excited by the unperturbed pressure. $p$ evaluated by Eq. (2a) is the perturbed pressure and specifically at $z=0$, it is called the surface pressure.

Upon splitting the incident pressure, $p_{\text{in}}$, from $p_{\text{unpt}}$, Eq. (2a) can be reexpressed as

$$p(x,z) = p_{\text{in}}(x,z) + p_{\text{scat}}(x,z), \tag{4a}$$

where

$$p_{\text{in}}(x,z) = P_{\text{inc}}e^{j\omega t - jkx\sin\theta + jkz\cos\theta}, \tag{4b}$$

$$p_{\text{scat}}(x,z) = P_{\text{inc}}e^{j\omega t - jkx\sin\theta - jkz\cos\theta} + p_{\text{rad}}(x,z). \tag{4c}$$

Equations (4a)–(4c) are similar to those for scattering by elastic objects,[40] where Eq. (4c) suggests that the interference of the reflected and radiated waves generates scattering. $p_{\text{scat}}$ is the scattered pressure which implicitly consists of the specularly reflected pressure of the baffle and the strip, and the diffracted pressure of the two ends of the strip due to discontinuities in acoustical impedance.

From the above description, it can be seen that Eqs. (2a) and (4a) provide two different physical interpretations of the perturbed wave. Equation (2a) describes the difference between the cases with and without the vibration of the strip, and the perturbed wave results when the radiated wave from the vibrating strip interferes with the propagating plane wave as if the strip is rigid. On the other hand, Eq. (4a) describes the difference between the cases with and without the boundary at $z=0$, and the perturbed wave results when the scattered wave from the baffle and the vibrating strip interferes with the incident wave. Although both equations yield the same $p$, the behaviors of $p_{\text{rad}}$ and $p_{\text{scat}}$ are different. Since the behavior of the radiated wave provides a direct indication of how the vibrating strip affects the unperturbed wave that is of interest in the present work, only Eqs. 2(a)–2(c), $p_{\text{unpt}}$, and $p_{\text{rad}}$ will be concerned in the following.

As the radiated wave is generated by the whole surface of the strip, $G$ can be defined as the Green's function at $(x,z)$ due to the radiation at $(x^{(s)},0)$, and it is given by[28,36,38]

$$G(x,z|x^{(s)},0) = jH^{(1,0)}[k\sqrt{(x-x^{(s)})^2+z^2}]/2, \tag{5}$$

where $H^{(1,0)}$ is the Hankel function of the first kind and zero order. By substituting Eqs. (3) and (5) into Eq. (2c), considering $\theta=90°$ in Eq. (2b) for a grazing incident plane wave that propagates from the left (see Fig. 1), and ignoring the alternating term, $e^{j\omega t}$, Eq. (2a) becomes

$$p(x,z) = 2P_{\text{inc}}e^{-jkx} - \frac{k}{2\zeta_L}\int_{-L/2}^{L/2} p(x^{(s)},0) \times H^{(1,0)}[k\sqrt{(x-x^{(s)})^2+z^2}]dx^{(s)}. \tag{6}$$

Given $P_{\text{inc}}$, $\zeta_L$, $k$, and $L$, Eq. (6) indicates that the surface pressure distribution of the strip is required if the perturbed pressure at any position on or above the baffle or the strip is to be calculated. As $H^{(1,0)}$ is within the integral and depends on $x^{(s)}$, it is obvious from the equation that an exact analytical solution of $p(x,z)$ cannot be obtained even when $p(x^{(s)},0)$ is known. So, other ways of solving $p(x,z)$ have been employed, such as the variational procedure and numerical procedures. However, in the variational procedure, it was still too difficult to derive a full solution, and only approximated solutions for high frequencies (large $k$) and lightly absorptive surfaces (large $\zeta_L$) have been obtained.[3,28,38] Thus, a numerical procedure called the quadrature technique[35,36,39] is used here.

### B. Solutions by the quadrature technique

In this technique, the strip is discretized into $M$ small elements of length $h$ (i.e., $L=Mh$). The total radiated pressure on the surface of the strip is then the sum of radiated pressures at all the discrete elements (i.e., at each element, the radiated pressure is the surface pressure weighted by a $kh/2\zeta_L$ factor and $H^{(1,0)}$). Mathematically, the integral in Eq. (6) is replaced by a summation over the $M$ elements and the equation is written as

$$\tilde{p}(x,z) = 2P_{\text{inc}}e^{-jkx} - \frac{kh}{2\zeta_L}\sum_{m=1}^{M}\tilde{p}(x_m^{(s)},0) \times H^{(1,0)}[k\sqrt{(x-x_m^{(s)})^2+z^2}], \tag{7}$$

where the tildes refer to approximated pressures because of the discretization. $x_m^{(s)}$ is taken as the $x$ coordinate at the midpoint of the $m$th element such that $x_m^{(s)}=-L/2+(m-1/2)h$ [i.e., $x_1^{(s)}=(-L+h)/2$ and $x_M^{(s)}=(L-h)/2$].

Since $\tilde{p}(x_m^{(s)},0)$ is still not known but required before $\tilde{p}(x,z)$ can be evaluated, Eq. (7) must first be used to solve the perturbed pressure at each element on the surface of the strip. Therefore, at the $n$th element, $x=x_n^{(s)}$ and $z=0$, and the equation becomes

$$\tilde{p}(x_n^{(s)},0) + \frac{kh}{2\zeta_L}\sum_{m=1}^{M}\tilde{p}(x_m^{(s)},0)H^{(1,0)}(k|x_n^{(s)}-x_m^{(s)}|) = 2P_{\text{inc}}e^{-jkx_n^{(s)}}. \tag{8}$$

It is apparent from Eq. (8) that for $n=m$ in which $x_n^{(s)}=x_m^{(s)}$, the argument of $H^{(1,0)}$ is zero [i.e., $H^{(1,0)}(0)$], where the Hankel function is undefined and the equation is singular. Hence, there are $M$ singularities for $n=1,\ldots,M$. Although this ill condition was mentioned in previous works,[36,39] exact ways of solving the problem have not been available for plane wave excitations. Even for spherical and cylindrical wave excitations, only an asymptotic way for large $k$ and $\zeta_L$ has been given.[36]

In order to avoid those singularities in the present work, a mean value of the Hankel function, $\bar{H}_{n,m}^{(1,0)}$, is chosen for use in the evaluation of the surface pressure at the $n$th element due to the radiation at the $m$th element. It is defined as the average of the two values of the Hankel function when both end points of the $m$th element are treated as the radiation points instead of its midpoint:

$$\bar{H}_{n,m}^{(1,0)} = [H^{(1,0)}(k|x_n^{(s)} - x_m^{(s1)}|) + H^{(1,0)}(k|x_n^{(s)} - x_{m+1}^{(s1)}|)]/2. \tag{9}$$

In Eq. (9), $x_m^{(s1)} = -L/2 + (m-1)h$ so that $x_1^{(s1)} = -L/2$, $x_{M+1}^{(s1)} = L/2$, and $x_m^{(s)} = (x_m^{(s1)} + x_{m+1}^{(s1)})/2$ (note: $x_m^{(s)}$ corresponds to the midpoint, and $x_m^{(s1)}$ and $x_{m+1}^{(s1)}$ correspond to the end points of the $m$th element). As $x_m^{(s)} \neq x_m^{(s1)}$ and $x_m^{(s)} \neq x_{m+1}^{(s1)}$, there are no singularities. Thus, Eq. (8) can be rewritten as

$$\tilde{p}(x_n^{(s)},0) + \frac{kh}{2\zeta_L}\sum_{m=1}^{M} \tilde{p}(x_m^{(s)},0)\bar{H}_{n,m}^{(1,0)} = p_{\text{unpt}}(x_n^{(s)},0), \tag{10}$$

where $p_{\text{unpt}}(x_n^{(s)},0) = 2P_{\text{inc}}e^{-jkx_n^{(s)}}$ is the unperturbed pressure at the $n$th element. If $M \to \infty$, then $h \to 0$, $x_m^{(s)} \approx x_m^{(s1)} \approx x_{m+1}^{(s1)}$, and $\tilde{p}(x_m^{(s)},0)$ for $m = 1, \ldots, M$ will approach the continuous distribution of the surface pressure of the strip, $p(x^{(s)},0)$.

By considering $M$ equations of the form of Eq. (10), a matrix equation can be constructed and the discrete surface pressure of the strip can be numerically solved as

$$\begin{bmatrix} \tilde{p}(x_1^{(s)},0) \\ \vdots \\ \tilde{p}(x_M^{(s)},0) \end{bmatrix} = \begin{bmatrix} 1 + kh\bar{H}_{1,1}^{(1,0)}/2\zeta_L & \cdots & kh\bar{H}_{1,M}^{(1,0)}/2\zeta_L \\ \vdots & \ddots & \vdots \\ kh\bar{H}_{M,1}^{(1,0)}/2\zeta_L & \cdots & 1 + kh\bar{H}_{M,M}^{(1,0)}/2\zeta_L \end{bmatrix}^{-1} \times \begin{bmatrix} p_{\text{unpt}}(x_1^{(s)},0) \\ \vdots \\ p_{\text{unpt}}(x_M^{(s)},0) \end{bmatrix}, \tag{11}$$

where $[\ ]^{-1}$ denotes the inverse of the matrix. Once the surface pressure distribution of the strip has been obtained, the radiated pressure at the $n$th element can be evaluated from the second term on the left-hand side of Eq. (10) as

$$\tilde{p}_{\text{rad}}(x_n^{(s)},0) = -\frac{kh}{2\zeta_L}\sum_{m=1}^{M} \tilde{p}(x_m^{(s)},0)\bar{H}_{n,m}^{(1,0)}. \tag{12}$$

In Eq. (12), a negative sign has been inserted because the radiated pressure was originally defined on the right-hand side of Eq. (2a). On the other hand, the radiated and perturbed pressures at elsewhere, $\tilde{p}_{\text{rad}}(x,z)$ and $\tilde{p}(x,z)$ for $z=0$ and $-\infty < x < -L/2$ or $L/2 < x < \infty$ (i.e., on the baffle), or $z > 0$ and $-\infty < x < \infty$ (i.e., above the baffle and the strip), can be calculated from Eq. (7). The radiated pressure is given by the last term in the equation as

$$\tilde{p}_{\text{rad}}(x,z) = -\frac{kh}{2\zeta_L}\sum_{m=1}^{M} \tilde{p}(x_m^{(s)},0)H^{(1,0)}[k\sqrt{(x-x_m^{(s)})^2 + z^2}]. \tag{13}$$

For any value of $\theta$, the complex sound intensity of the strip at $(x_m^{(s)},0)$ in the $z$ direction is written as

$$I_z(x_m^{(s)}) = -\tilde{p}(x_m^{(s)},0)\tilde{v}^*(x_m^{(s)})/2 = -|\tilde{p}(x_m^{(s)},0)|^2/2\rho_0 c_0 \zeta_L^*, \tag{14}$$

where $\tilde{v}(x_m^{(s)})$ $[=\tilde{p}(x_m^{(s)},0)/\rho_0 c_0 \zeta_L]$ is the normal velocity of the surface of the strip and the asterisk (*) denotes the complex conjugate. The negative sign in Eq. (14) indicates that the normal intensity flow into the strip is opposite to the $z$ direction. From this equation, the surface intensity can be evaluated when the surface pressure and impedance of the strip are known. The sound absorption coefficient of the strip can then be obtained as

$$\alpha_L = \frac{1}{M}\sum_{m=1}^{M} \text{Re}[I_z(x_m^{(s)})]/-|P_{\text{inc}}|^2 \cos\theta/2\rho_0 c_0, \tag{15}$$

where Re[ ] denotes the real part of the complex quantity. The numerator on the right-hand side of Eq. (15) describes the spatial average real intensity (or absorbed sound power per unit length) of the strip. The denominator with a negative sign represents the intensity of the incident plane wave in the direction which is normal to the strip and opposite to the $z$ direction.

When $\theta = 90°$ as is of interest here, it is obvious from Eq. (15) that the denominator becomes zero (due to $\cos\theta = 0$) and for any nonzero finite value of the numerator, $\alpha_L$ is infinite. In other words, when the definition of $\alpha_L$ in Eq. (15) is employed, $\alpha_L$ cannot describe the sound absorptivity of the strip for the excitation at grazing incidence. However, since $\theta$ is fixed throughout the present work because only $\theta = 90°$ is considered, the full intensity of the incident wave in the propagation direction (i.e., $-|P_{\text{inc}}|^2/2\rho_0 c_0$) can be reasonably used as a comparative measure for the extent of absorbed (real part) intensity of the strip. The absorption coefficient can then be redefined to provide a description of the absorptivity of the strip, and it is given by

$$\alpha_L = \frac{1}{M}\sum_{m=1}^{M} \text{Re}[I_z(x_m^{(s)})]/-|P_{\text{inc}}|^2/2\rho_0 c_0. \tag{16}$$

As will be shown later in Sec. III B, Eq. (16) gives $\alpha_L = 0$ (the strip does not absorb sound) when the length of the strip is infinite. Therefore, this definition of $\alpha_L$ is also consistent with Eq. (1) that an infinite impedance surface does not absorb sound when $\theta = 90°$.

## III. RESULTS AND DISCUSSION

In the following, examples are presented to illustrate the effects of the radiated wave on the distributions of surface pressure and absorbed intensity of the strip for a grazing incident plane wave. The influence of the surface intensity distribution on the absorption coefficient of the strip is also revealed. From Eq. (10), as $\tilde{p}(x_n^{(s)},0)$ is dependent on $p_{\text{unpt}}(x_n^{(s)},0)$ that has the $e^{-jkx_n^{(s)}}$ term, the surface pressure solved by Eq. (11) will alternate in terms of $kx$, and the variations with $k$ and $L$ are the same for the surface pressure and intensity. In addition, for a given $P_{\text{inc}}$ and $\zeta_L$, the surface pressure and the intensity do not change with $k$ and $L$ as long as $kL$ is the same. So, in the examples, $P_{\text{inc}} = 1.0$ Pa and $L = 3$ m are used, $\zeta_L$ and $k$ are altered, but $kL$ is quoted.

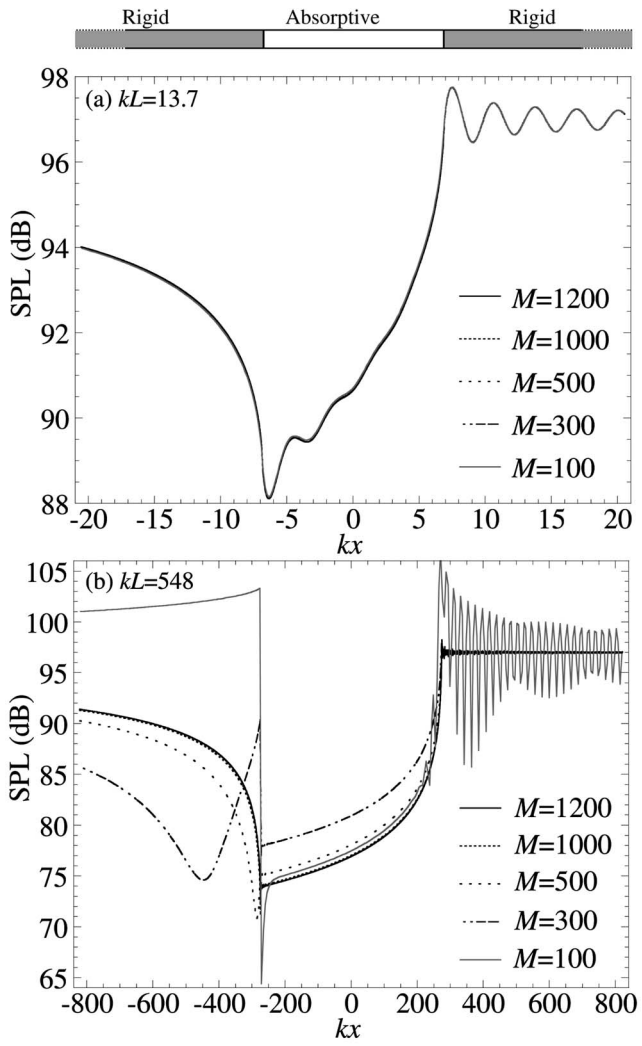


FIG. 2. Distributions of perturbed sound pressure level at $z=0$ for $P_{inc}=1.0$ Pa, $\zeta_L=0.2-j2$, and five different values of $M$. (a) $kL=13.7$ and (b) $kL=548$.

### A. Convergence of surface pressure of the strip

As far as discretization is concerned, it is known that there must be at least four discrete elements within a wavelength, λ, for the frequency of a sinusoidal wave to be accurately identified (i.e., discretize the surface of the strip at quarter wavelengths). Mathematically, the corresponding length of each element, $h_{conv}$, and the number of elements, $M_{conv}$, are such that $h_{conv}=\lambda/4$ (or $L/M_{conv}=\pi/2k$), which implies $M_{conv}=2kL/\pi$. In this case, $M_{conv}$ only provides a rough indication of the onset of convergence of the surface pressure of the strip [thus, the convergences of the radiated pressure and intensity on the surface of the strip from Eqs. (12) and (14), and the perturbed and radiated pressures at elsewhere from Eqs. (7) and (13)]. Hence, $M \gg 2kL/\pi$ if a perturbed or radiated wave with a fully converged pressure is to be obtained. As a result, a greater $M$ is required for a larger $kL$.

Figure 2 depicts the distributions of perturbed sound pressure level (SPL) at $z=0$ for five different values of $M$, $\zeta_L=0.2-j2$, and $f=250$ Hz and 10 kHz (i.e., $kL=13.7$ and 548, and correspondingly, $M_{conv}\approx 9$ and 349). When $kL$ is small, λ is large compared to $L$, and the surface pressure of the strip varies slowly with distance such that a low resolution of discretization (i.e., small $M$ or large $h$ since $h=L/M$) is adequate. As an example, Fig. 2(a) shows that for the small $kL$ of 13.7, the perturbed SPL has already converged even when $M=100$ ($\gg M_{conv}$ of 9), and a further increase in $M$ does not produce any distinguishable change in the pressure distribution. When $kL$ is large, λ is small compared to $L$, and the surface pressure of the strip varies rapidly with distance. A high resolution of discretization (i.e., large $M$ or small $h$) is thus required to avoid losing details of the pressure within small intervals on the surface. For example, as shown in Fig. 2(b) for the large $kL$ of 548, there are still considerable errors in the perturbed SPL when $M=100$ or even 300 ($<M_{conv}$ of 349). It is also evident that the entire SPL distribution has already started to converge when $M=500$, and a complete convergence can be achieved only when $M>1000$. As the discretization is only related to $kL$, $\zeta_L$ does not affect the convergences of the perturbed and radiated pressures, and the surface intensity of the strip. So, the value of $M$ is selected on the basis that the surface pressure of the strip has already well converged for a given $kL$. In the following, based on a full convergence of this surface pressure for $kL=548$ which is the largest value considered, $M=1500$ is used for all values of $kL\leq 548$ and is well sufficient.

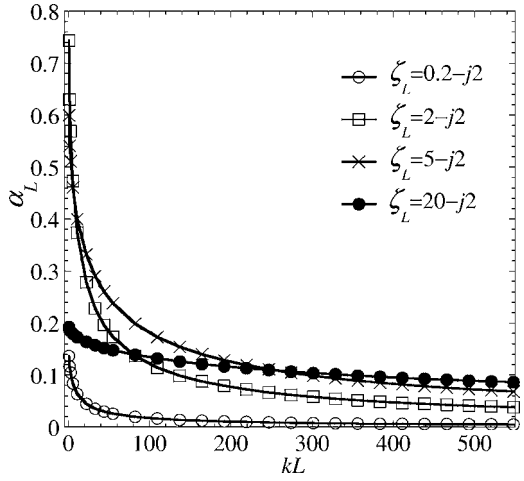


FIG. 3. Sound absorption coefficient of the strip vs $kL$ for four different values of $\zeta_L$.

### B. Sound absorption coefficient of the strip

$\alpha_L$ vs $kL$ for four different values of $\zeta_L$ is presented in Fig. 3, and two important features can be drawn from the figure. First, $\alpha_L$ is clearly nonzero (the strip absorbs sound) and different for different values of $\zeta_L$ even though the incident wave is a grazing plane wave. The variation of $\alpha_L$ with $kL$ resembles an exponential decay (although it is not) where $\alpha_L$ decreases rapidly with $kL$. Due to this trend of variation, for any of the values of $\zeta_L$ shown, $\alpha_L$ is higher for a low frequency and a short strip than for a high frequency and a long strip. Also, $\alpha_L=0$ only if $kL\to\infty$ when the frequency and/or length of the strip is infinite. The latter case is consistent with Eq. (1) for an infinite impedance surface, which

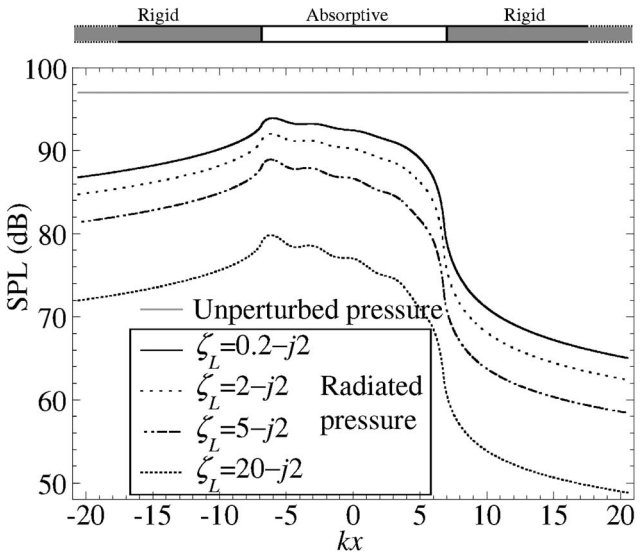


FIG. 4. Distributions of unperturbed and radiated sound pressure levels at $z=0$ for $P_{\text{inc}}=1.0$ Pa, $kL=13.7$, and four different values of $\zeta_L$.

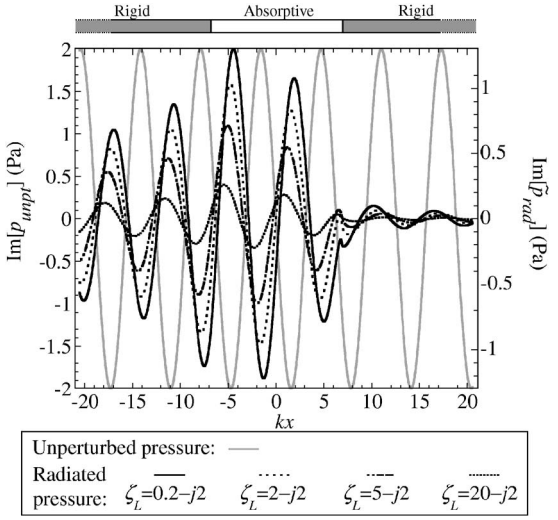


FIG. 5. Imaginary parts of the unperturbed and radiated sound pressures at $z=0$ for $P_{\text{inc}}=1.0$ Pa , $kL=13.7$, and four different values of $\zeta_L$. Im[ ] denotes the imaginary part of the complex quantity.

gives a zero absorption coefficient ($R_L=-1$) for $\theta=90°$ even when $\zeta_L$ is finite and nonzero. As far as the second feature is concerned, in general, $\alpha_L$ for $kL<10$ is highest when the real part of $\zeta_L$ is close to 1, where the resistance (real part of impedance) of the strip is close to the characteristic impedance of air (i.e., in Fig. 3, at the first four values of $kL<10$, $\alpha_L$ is highest for $\zeta_L=2-j2$, followed by $\zeta_L=5-j2$, $20-j2$, and $0.2-j2$). However, it can be seen from the figure that $\alpha_L$ decreases with $kL$ more rapidly for a small $\zeta_L$ than for a large $\zeta_L$. As a result, $\alpha_L$ is eventually higher for a large $\zeta_L$ than for a small $\zeta_L$ (e.g., from $kL>10$ onwards, $\alpha_L$ is higher for $\zeta_L=5-j2$ than for $\zeta_L=2-j2$, from $kL>80$ onwards, $\alpha_L$ is higher for $\zeta_L=20-j2$ than for $\zeta_L=2-j2$, and from $kL>270$ onwards, $\alpha_L$ is higher for $\zeta_L=20-j2$ than for $\zeta_L=5-j2$). The above-mentioned two features of $\alpha_L$ are consecutively explained in the following, where the behavior of the radiated wave on the surface of the strip and the effect of the radiated pressure on the surface absorption of the strip are described in detail. The case of a small $kL$ is first illustrated.

### C. Variations of pressures and intensity with $\zeta_L$

Figure 4 presents the distributions of radiated SPL at $z=0$ for $kL=13.7$ and the four values of $\zeta_L$ as before. Also shown is the uniform distribution of unperturbed SPL that is associated with the unperturbed wave. The radiation of the strip is stronger if the impedance difference between the strip and the baffle is greater (i.e., smaller $\zeta_L$ since the baffle has an infinite impedance) [note: From Eq. (12) or (13), $\tilde{p}_{\text{rad}} \propto 1/\zeta_L$]. Therefore, the radiated SPL is lowest for $\zeta_L=20-j2$ and highest for $\zeta_L=0.2-j2$, and it converges toward the unperturbed SPL as $\zeta_L$ decreases (see Fig. 4). When the plane wave propagates from the left baffle to the strip, it is strongly perturbed by a sudden change to a finite impedance at the baffle-strip interface where a strong radiation of the strip is induced. As there are no discontinuities in impedance when the plane wave propagates along the strip, the perturbation reduces gradually across the strip and a decreasing radiation is induced. When the plane wave propagates from the strip to the right baffle, the perturbation is further reduced by a sudden change back to an infinite impedance at the strip-baffle interface where the radiation of the strip is thus considerably weak. Consequently, it is obvious from Fig. 4 that when one proceeds from the left baffle to the strip, the radiated SPL increases until a maximum value at the baffle-strip interface. Then, it decreases slowly across the strip and exhibits a sharp drop around the strip-baffle interface after which a slow drop continues. This radiated pressure interferes with the unperturbed pressure, so the superposition of the radiated and unperturbed waves on the surfaces of the baffle and the strip is now examined.

Recall that $\tilde{p}(x_n^{(s)},0)$ obtained from Eq. (11) alternates in terms of $kx$ because $p_{\text{unpt}}(x_n^{(s)},0)$ has the $e^{-jkx_n^{(s)}}$ term. From Eq. (12) or (13), $\tilde{p}_{\text{rad}}$ is dependent on $\tilde{p}(x_n^{(s)},0)$, and it follows that $\tilde{p}_{\text{rad}}$ also alternates in terms of $kx$. The alternating manner of $p_{\text{unpt}}$ and $\tilde{p}_{\text{rad}}$ is described in their real and imaginary parts. Both parts are similar in wave form but different by 90° in phase, and they provide similar information of the pressures. Hence, only the imaginary parts of $p_{\text{unpt}}$ and $\tilde{p}_{\text{rad}}$ at $z=0$ are presented in Fig. 5 for the same conditions as in Fig. 4. From Fig. 5, the unperturbed pressure has a constant amplitude that produces the uniform distribution of the unperturbed SPL in Fig. 4. Also, the amplitude of the radiated pressure decreases with $\zeta_L$ in Fig. 5, which corresponds to the drop of the radiated SPL with $\zeta_L$ observed in Fig. 4. Since the unperturbed wave is for the case as if the strip is rigid (i.e., $\zeta_L \to \infty$), in general, the unperturbed and radiated pressures are in phase to each other if the impedance difference between the strip and the baffle is small (i.e., large $\zeta_L$), and out of phase if the impedance difference is large (i.e., small $\zeta_L$). However, when $\zeta_L$ is large, the radiation of the strip will not have any significant influence on the unperturbed wave because the radiated pressure is negligibly low compared to the unperturbed pressure. In other words, $\zeta_L$ has to be small for the radiated pressure to be comparable to the unperturbed pressure (which is immediately clear from Figs. 4 and 5),

where both pressures are consequently out of phase to each other. Thus, as can be seen in Fig. 5 for all the values of $\zeta_L$ shown, the unperturbed and radiated waves superimpose out of phase. It is also evident that the latter shifts gradually as $\zeta_L$ increases, and its phase difference to the former slowly reduces. Hence, the phase difference between the unperturbed and radiated pressures is large when $\zeta_L$ is small (e.g., $\zeta_L=0.2-j2$, $2-j2$, and $5-j2$ in Fig. 5 where the pressures are mainly close to 180° out of phase to each other), and small when $\zeta_L$ is large (e.g., $\zeta_L=20-j2$ in Fig. 5 where the pressures are mainly away from 180° out of phase).

Figure 6 shows the distributions of perturbed SPL at $z=0$ (i.e., surface pressure) after the radiated and unperturbed waves have been superimposed. By comparing these distributions to those in Fig. 4, it can be seen that the behavior of the perturbed SPL is opposite to that of the radiated SPL, because the unperturbed and radiated waves superimpose out of phase as has been shown in Fig. 5 (i.e., the surface pressure is high when the radiated pressure is low and vice versa). For example, the surface pressure throughout the strip is highest for $\zeta_L=20-j2$ and lowest for $\zeta_L=0.2-j2$. At the baffle-strip interface where the maximum of the radiated SPL occurs, a minimum surface pressure is found. Also, around the strip-baffle interface where the sharp drop of radiated SPL occurs, a rapid increase of surface pressure is observed (compare Figs. 4 and 6). Since the radiated pressure is higher for a lower $\zeta_L$, it affects the unperturbed pressure considerably more for a low $\zeta_L$ than for a high $\zeta_L$. So, although the slopes of decrease in radiated SPL over the strip are almost the same for all four values of $\zeta_L$ (see Fig. 4), Fig. 6 indicates that the slopes of increase in surface pressure over the strip are substantially different (i.e., steepest for $\zeta_L=0.2-j2$, followed by $\zeta_L=2-j2$, $5-j2$, and $20-j2$). This surface pressure distribution determines two acoustical aspects of the strip, namely, the profile of the plane wave front above the strip and the absorbed intensity distribution on the surface of the strip.

In order to visualize the radiated wave effect on the profile of the plane wave front, the perturbed SPL at $z>0$ is also evaluated for the same conditions as in Fig. 6. Figure 7 shows the distributions of perturbed SPL on and above the baffle and the strip at five locations. Two of the locations are above the baffle (before the baffle-strip interface and after the strip-baffle interface), and the other three locations are above the strip (at the middle of the strip and in the vicinity of both interfaces). As $\tilde{p}(x,z)$ depends on $\tilde{p}(x_m^{(s)},0)$ and $H^{(1,0)}$ in Eq. (7), and the magnitude of $H^{(1,0)}$ is large when $kz \ll 1$, the perturbed pressure at $z>0$ around the strip is close to the surface pressure of the strip and hence, deviates from the unperturbed pressure [note: In Eq. (7), $\tilde{p}(x_m^{(s)},0)$ is weighted by $H^{(1,0)}$]. The perturbed pressure approaches the unperturbed pressure when $kz$ increases because the magnitude of $H^{(1,0)}$ reduces with $kz$ [i.e., the value of the last term in Eq. (7) that describes the radiated pressure, reduces with $kz$]. As a result of the deviation from the unperturbed pressure, pressure curvatures are generated on the perturbed wave and the plane wave front becomes distorted. The distortion of the propagating plane wave is clearly shown in Fig. 7 for the four values of $\zeta_L$, where the curvature of the wave front is

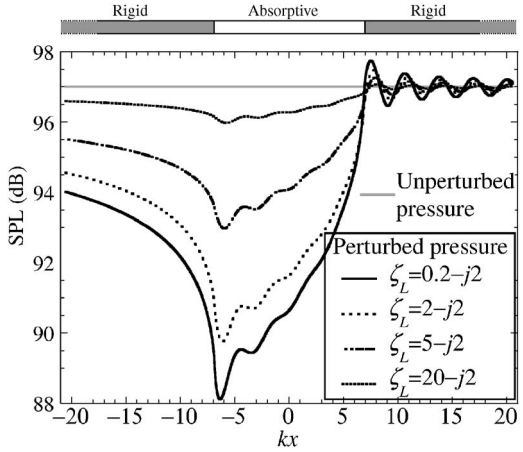


FIG. 6. Distributions of unperturbed and perturbed sound pressure levels at $z=0$ for $P_{\text{inc}}=1.0$ Pa, $kL=13.7$, and four different values of $\zeta_L$.

large on and near the surfaces of the baffle and the strip, but decreases with the distance from the surfaces (i.e., $z$). Since the discrepancy between the perturbed and unperturbed SPLs in Fig. 6 reduces with $\zeta_L$, the distortion also decreases with $\zeta_L$ [e.g., from Figs. 7(a) to 7(d), the distortion is largest for $\zeta_L=0.2-j2$, followed by $\zeta_L=2-j2$, $5-j2$, and $20-j2$]. Following the observations in Figs. 4 and 6, Fig. 7 also indicates that when one proceeds from the left baffle to the strip, the distortion increases to the largest at the baffle-strip interface, decreases gradually across the strip, and finally becomes insignificant around the strip-baffle interface and beyond. In other words, the surface pressure and the profile of the plane wave front in the vicinity of the baffle-strip interface are most significantly affected by the radiation of the strip.

Due to the nonzero surface pressure of the strip, which varies with $\zeta_L$ and has a nonuniform distribution as in Fig. 6, the absorbed intensity on the surface of the strip is also nonzero, varies with $\zeta_L$, and has a nonuniform distribution as depicted in Fig. 8 [note: From Eq. (14), the surface intensity is directly proportional to the surface pressure]. This explains the first feature from Fig. 3 that $\alpha_L$ is nonzero and different for the four values of $\zeta_L$. It can be seen from Fig. 8 that the slope of increase in intensity over the strip drops with $\zeta_L$, which is caused by the similar variation of the slope of increase in surface pressure over the strip with $\zeta_L$ (see Fig. 6). So, the surface absorption of the strip is highly and most nonuniform for $\zeta_L=0.2-j2$, but nearly and most uniform for $\zeta_L=20-j2$. In addition, the intensity is lowest around the baffle-strip interface that has the maximum radiated pressure, and increases across the strip until a maximum value at the strip-baffle interface that has the minimum radiated pressure. As the product of the surface pressure and $\text{Re}[1/\zeta_L^*]$ is largest for $\zeta_L=5-j2$ and smallest for $\zeta_L=0.2-j2$ {i.e., from Eq. (14), $\text{Re}[I_z(x_m^{(s)})] \propto |\tilde{p}(x_m^{(s)},0)|^2 \text{Re}[1/\zeta_L^*]$ can be deduced}, the overall absorbed intensity is highest for $\zeta_L=5-j2$, followed by $\zeta_L=2-j2$, $20-j2$, and $0.2-j2$ (see Fig. 8). So, at $kL=13.7$, $\alpha_L$ is higher for $\zeta_L=5-j2$ than for $\zeta_L=2-j2$ as observed in Fig. 3.

### D. Variations of pressures and intensity with *kL*

In this section, the radiated wave effect for larger values of $kL$ is considered. Generally, the plane wave for a larger $kL$

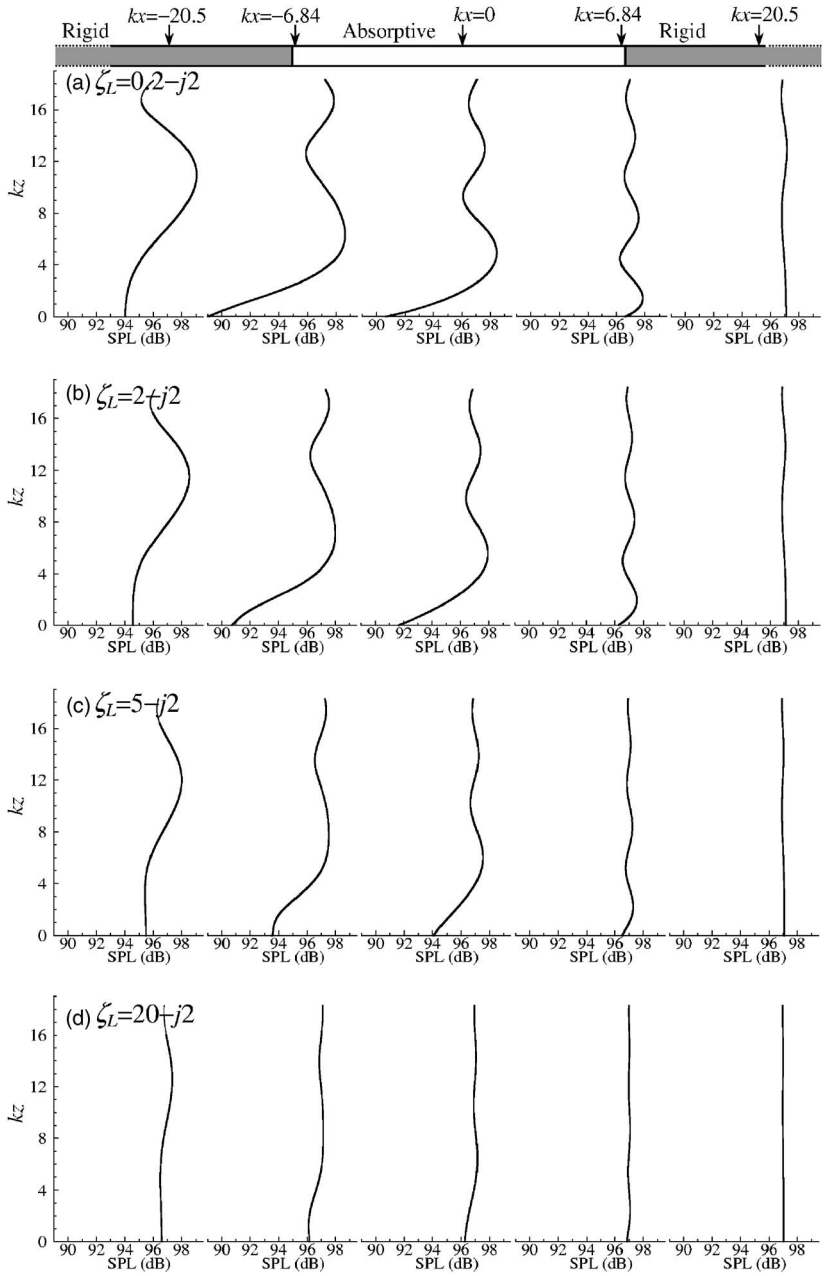


FIG. 7. Distributions of perturbed sound pressure level at $kx=-20.5$, $-6.84$, 0, 6.84, and 20.5 for $P_{\text{inc}}=1.0$ Pa, $kL=13.7$, and (a) $\zeta_L=0.2-j2$, (b) $\zeta_L=2-j2$, (c) $\zeta_L=5-j2$, and (d) $\zeta_L=20-j2$.

is easier to perturb because of a shorter λ compared to $L$, where a stronger radiation of the strip is induced. The radiated pressure is then higher and more uniform for a large $kL$ than for a small $kL$ [note: From Eq. (12) or (13), $\tilde{p}_{\text{rad}} \propto kh \propto kL$]. Consequently, when the perturbation of the plane wave near the strip-baffle interface is greatly reduced by a sudden change to an infinite impedance, the drop in the radiation of the strip around this discontinuity in impedance is shaper for the large $kL$. This phenomenon is illustrated in Fig. 9, which provides a comparison of radiated SPL at $z=0$ for $\zeta_L=2-j2$ and $20-j2$, and $kL=13.7$, 43.8, and 137 (i.e., associated with $f=250$, 800, and 2500 Hz for $L=3$ m). It is obvious that for both values of $\zeta_L$, the sharp drop of radiated SPL in the proximity of the strip-baffle interface, increases with $kL$. The radiated SPL on the left baffle around the baffle-strip interface and on most of the length of the strip, also increases and converges toward the unperturbed SPL as $kL$ increases [compare Figs. 9(a)–9(c)].

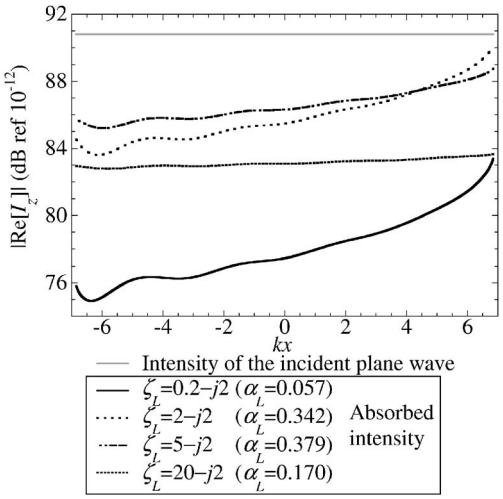


FIG. 8. Distributions of the intensity of the incident plane wave and absorbed intensity on the surface of the strip for $P_{\text{inc}}=1.0$ Pa, $kL=13.7$, and four different values of $\zeta_L$.

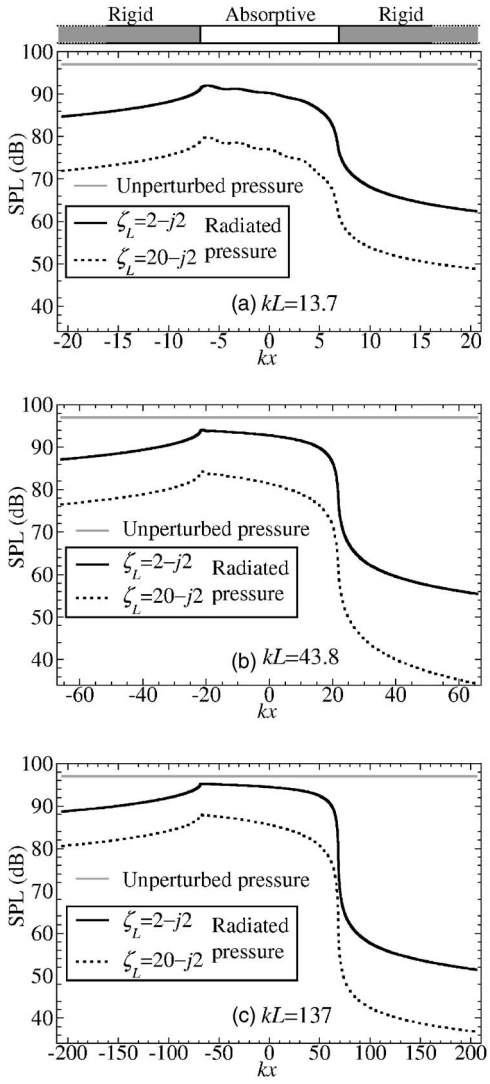


FIG. 9. Distributions of unperturbed and radiated sound pressure levels at $z=0$ for $P_{inc}=1.0$ Pa, $\zeta_L=2-j2$ and $20-j2$, and (a) $kL=13.7$, (b) $kL=43.8$, and (c) $kL=137$.

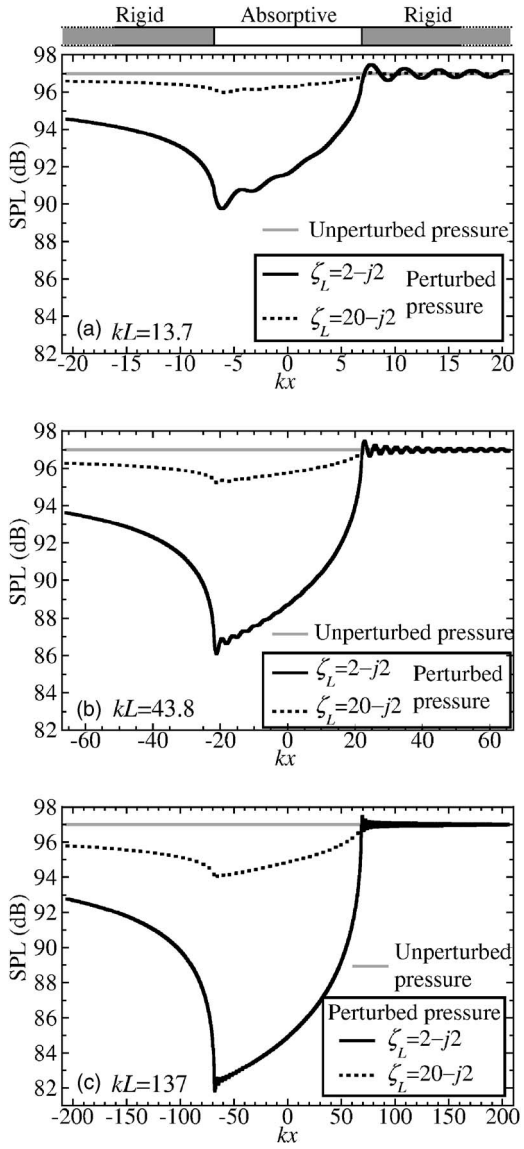


FIG. 10. Distributions of unperturbed and perturbed sound pressure levels at $z=0$ for $P_{inc}=1.0$ Pa, $\zeta_L=2-j2$ and $20-j2$, and (a) $kL=13.7$, (b) $kL=43.8$, and (c) $kL=137$.

As a result of the behavior of the radiated SPL in Fig. 9 as well as the above-mentioned out-of-phase superposition between the unperturbed and radiated waves, Figs. 10(a)–10(c) show that only the surface pressure of the strip and the right baffle around the strip-baffle interface is nearly unchanged with $kL$ and close to the unperturbed pressure. Although the slope of increase in surface pressure over the strip rises considerably with $kL$, the surface pressure of the left baffle near the baffle-strip interface and of a large extent of the strip substantially decreases away from the unperturbed pressure. As the radiated SPL is much closer to the unperturbed SPL for $\zeta_L=2-j2$ than for $\zeta_L=20-j2$ (see Fig. 9), Fig. 10 indicates that the surface pressure for the low $\zeta_L$ decreases much faster with $kL$ than that for the high $\zeta_L$. Due to the deviation of the perturbed pressure from the unperturbed pressure, being smallest for $kL=13.7$ and largest for $kL=137$, the pressure curvature of the wave front on and near the surfaces of the baffle around both interfaces and of the strip is smallest for $kL=13.7$ and largest for $kL=137$. As an example for $\zeta_L=2-j2$, Figs. 11(a)–11(c) indicate that the distortion of the propagating plane wave is smallest for $kL=13.7$, followed by $kL=43.8$ and 137. Following the observations in Figs. 9 and 10 for $\zeta_L=2-j2$, it is also apparent in Fig. 11 that for all three values of $kL$, the profile of the plane wave front in the proximity of the baffle-strip interface is most significantly affected by the radiation of the strip.

Figure 12 shows the absorbed intensity of the strip for the same conditions as in Figs. 9–11. For both values of $\zeta_L$, the intensity reduces with $kL$ [compare Figs. 12(a)–12(c)] because the surface pressure decreases with $kL$ (see Fig. 10). From this trend, it can be deduced that in the limit of $kL \rightarrow \infty$, the surface pressure and thus the intensity will tend to zero [i.e., corresponds to the radiated SPL that tends to the unperturbed SPL as in Figs. 9(a)–9(c), as well as the out-of-phase superposition between the radiated and unperturbed waves]. This explains the reason for the decreasing trend of $\alpha_L$ with $kL$ that eventually leads to $\alpha_L=0$ when $kL \rightarrow \infty$, which is also the first feature from Fig. 3. The decrease of the surface pressure but the rise of the slope of increase in surface pressure over the strip with $kL$ are faster for $\zeta_L=2-j2$

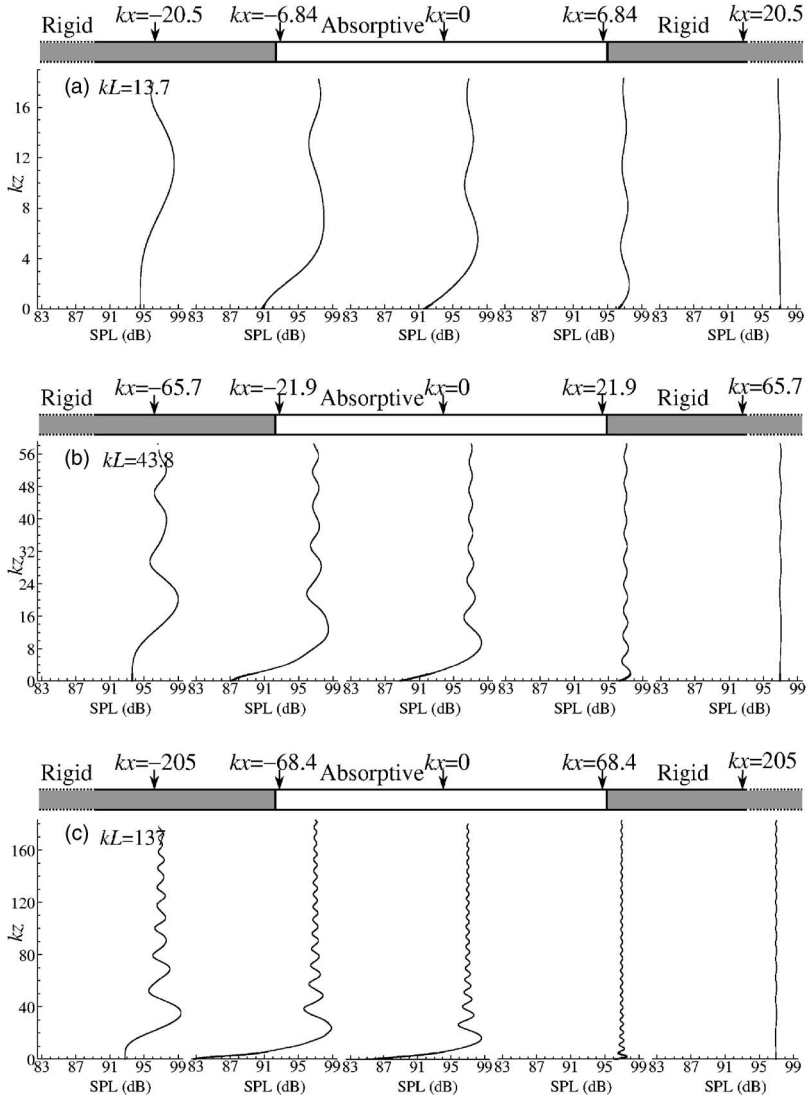


FIG. 11. Distributions of perturbed sound pressure level at $kx=-20.5$, $-6.84$, 0, 6.84, and 20.5 for $P_{\text{inc}}=1.0$ Pa, $\zeta_L=2-j2$, and (a) $kL=13.7$, (b) $kL=43.8$, and (c) $kL=137$.

than for $\zeta_L=20-j2$ (see Fig. 10). Hence, the product of the surface pressure and $\text{Re}[1/\zeta_L^*]$ (i.e., absorbed intensity), which is lower for $\zeta_L=20-j2$ than for $\zeta_L=2-j2$ at $kL=13.7$, becomes higher for the large $\zeta_L$ than for the small $\zeta_L$ at $kL=137$. For example, as can be seen in Fig. 12(a) for $kL=13.7$, the absorbed intensity throughout the strip and thus $\alpha_L$ are lower for $\zeta_L=20-j2$. When $kL$ increases to 43.8, the intensity on the left half of the strip is higher for $\zeta_L=20-j2$ than for $\zeta_L=2-j2$, and the values of $\alpha_L$ for both values of $\zeta_L$ are close to each other [see Fig. 12(b)]. At $kL=137$, the intensity for $\zeta_L=20-j2$ is higher across most of the length of the strip, so $\alpha_L$ for $\zeta_L=20-j2$ becomes greater than that for $\zeta_L=2-j2$ [see Fig. 12(c)]. This behavior of the intensity explains the second feature from Fig. 3 that although $\alpha_L$ is lower for a large $\zeta_L$ than for a small $\zeta_L$ at a small $kL$, it can become greater for the former than for the latter at a large $kL$. The intensity distributions also suggest that a greater $\alpha_L$ for one value of $\zeta_L$ does not mean that the surface absorption across the entire strip is also larger than that for the other value of $\zeta_L$ [e.g., for $\zeta_L=20-j2$ in Fig. 12(b), $\alpha_L$ is lower but the intensity is higher on the baffle-strip interface side, and for $\zeta_L=2-j2$ in Fig. 12(c), $\alpha_L$ is lower but the intensity is higher around the strip-baffle interface].

## IV. CONCLUSIONS

In this paper, characteristics of sound pressure and intensity on the surface of a finite impedance strip flush-mounted on a rigid baffle are studied for a plane wave excitation at grazing incidence. The boundary integral method is used, where the surface pressure of the strip is expressed in terms of the superposition between the unperturbed wave and the radiated wave from the strip (the total is called the perturbed wave). In order to avoid singularities in the numerical solutions of the surface pressure, the quadrature technique used to solve the boundary integral problem after the discretization of the strip into $M$ small elements is modified by defining a mean value of Hankel function for each element. This mean value is the average of the two values of the Hankel function as when both end points (rather than the midpoint) of the element are treated as the radiation points. The solutions are well converged only when $M \gg 2kL/\pi$. A single value of $M$ is used for all values of $kL$ considered here, and it is based on a full convergence of the surface pressure of the strip for the largest of those values of $kL$.

The radiated pressure is highest at the baffle-strip interface, reduces across the strip, and is considerably low around

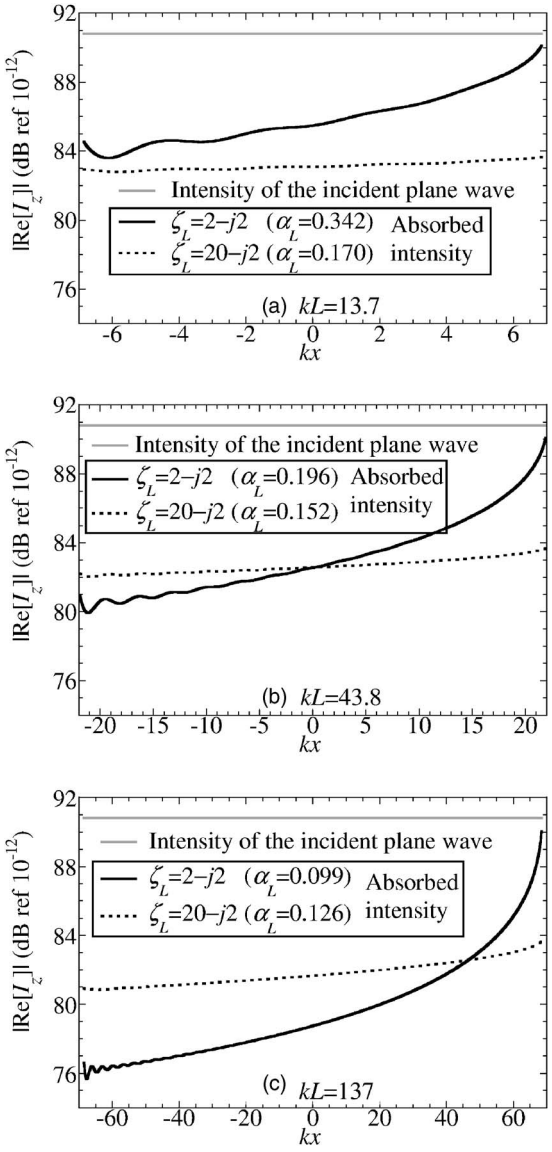


FIG. 12. Distributions of the intensity of the incident plane wave and absorbed intensity on the surface of the strip for $P_{inc}$=1.0 Pa, $\zeta_L$=2−$j$2 and 20−$j$2, and (a) $kL$=13.7, (b) $kL$=43.8, and (c) $kL$=137.

the strip-baffle interface. Throughout most of the length of the strip, the radiated pressure decreases with $\zeta_L$ and increases with $kL$, but around the strip-baffle interface, it decreases with both $\zeta_L$ and $kL$. Since the unperturbed and radiated waves have different magnitudes and superimpose out of phase, the surface pressure of the strip is lowest at the baffle-strip interface and increases across the strip. It also increases with $\zeta_L$ and decreases with $kL$, except around the strip-baffle interface where it is nearly unchanged and close to the unperturbed pressure. Due to the deviation of the perturbed pressure on and above the surface of the strip from the unperturbed pressure, pressure curvatures are generated on the perturbed wave and the plane wave front becomes distorted. The distortion is large on and near the surface, but reduces with the distance from the surface. It is also largest at the baffle-strip interface, and reduces gradually toward the strip-baffle interface where it becomes very small. In other words, the surface pressure of the strip and the profile of the plane wave front near the baffle-strip interface are most significantly affected by the radiation of the strip. As the surface intensity is directly proportional to the surface pressure, the absorbed intensity of the strip is lowest around the baffle-strip interface and increases across the strip, where the slope of the increase (i.e., the nonuniformity of the intensity distribution) drops with $\zeta_L$ but rises with $kL$. Therefore, the intensity is nonzero, and varies with $\zeta_L$ and $kL$. Hence, $\alpha_L$ is also nonzero, and different for different values of $\zeta_L$ and $kL$. The decreasing trend of the surface pressure with $kL$ implies that in the limit of $kL \to \infty$, the intensity will approach zero, which eventually leads to $\alpha_L=0$. As the intensity across a large extent of the strip decreases with $kL$ faster for a small $\zeta_L$ than for a large $\zeta_L$, the spatial average intensity over the entire strip (thus, $\alpha_L$) for the small $\zeta_L$, which is initially higher at a small $kL$, can become lower than that for the large $\zeta_L$ at a large $kL$.

In order to experimentally measure the distortion of a grazing plane wave front by an impedance strip as well as the distribution of surface intensity and resulting absorption coefficient of the strip, the incident wave needs to be planar and exactly graze the strip. Such excitation is very prone to errors, and the difficulty of its precise arrangement was obvious from previous measurements of impedance and/or absorption coefficient, which could only consider excitations that were far from grazing incidence for the incident wave to be planar.[9,32] Even when the incident wave was spherical, excitations could only be considered up to near grazing incidence.[7,18–20] So, in the case of a grazing plane wave as concerned here, it is necessary to discuss in detail the issues of deviation of the incident wave from planar and deviation of the excitation from grazing incidence. The effects of these deviations on the measured pressure, surface intensity, and absorption coefficient also need to be quantified, and the experiment is separately considered as a future work. Since the boundary integral method used here relies on the Green's function of the sound field, it can be further developed for predicting the size/edge effects of finite boundaries on the decay times of acoustic modes in ordinary rooms where the sound fields are not diffuse.

Given the great interest in the development of techniques for predicting impedances of absorptive materials in recent years, it is also important to establish some guidelines on the impact of edge diffraction (due to discontinuities in impedance) on the *in situ* measurement of impedance. For this purpose, one not only needs to deal with the grazing angle as concerned here, but also the normal and oblique angles as well as various materials of different absorptions and sizes (or frequencies) for these nongrazing angles. The reason is because the diffraction changes with any of these parameters. Although such investigation is beyond the scope of this paper, it could be useful as a future work.

[1]P. M. Morse and R. H. Bolt, "Sound waves in rooms," Rev. Mod. Phys. **16**, 69–150 (1944).
[2]H. Kuttruff, "The sound field in front of a wall," in *Room Acoustics*, 2nd ed. (Applied Science, London, 1979), Chap. 2, pp. 20–43.
[3]S. Thomasson, "On the absorption coefficient," Acustica **44**, 265–273 (1980).
[4]F. V. Hunt, L. L. Beranek, and D. Y. Maa, "Analysis of sound decay in

rectangular rooms," J. Acoust. Soc. Am. **11**, 80–94 (1939).
[5]B. Yegnanarayana, "Wave analysis of sound decay in rectangular rooms," J. Acoust. Soc. Am. **56**, 534–541 (1974).
[6]B. Yegnanarayana and B. S. Ramakrishna, "Diffusion of decaying sound field in a reverberation room with a highly absorbing sample," J. Acoust. Soc. Am. **56**, 706–708 (1974).
[7]C. Klein and A. Cops, "Angle dependence of the impedance of a porous layer," Acustica **44**, 258–264 (1980).
[8]M. Tamura, "Spatial Fourier transform method of measuring reflection coefficients at oblique incidence. I. Theory and numerical examples," J. Acoust. Soc. Am. **88**, 2259–2264 (1990).
[9]J. F. Li and M. Hodgson, "Use of pseudo-random sequences and a single microphone to measure surface impedance at oblique incidence," J. Acoust. Soc. Am. **102**, 2200–2210 (1997).
[10]J. S. Suh and P. A. Nelson, "Measurement of transient response of rooms and comparison with geometrical acoustic models," J. Acoust. Soc. Am. **105**, 2304–2317 (1999).
[11]I. Rudnick, "The propagation of an acoustic wave along a boundary," J. Acoust. Soc. Am. **19**, 348–356 (1947).
[12]R. B. Lawhead and I. Rudnick, "Acoustic wave propagation along a constant normal impedance boundary," J. Acoust. Soc. Am. **23**, 546–549 (1951).
[13]C. F. Chien and W. W. Soroka, "Sound propagation along an impedance plane," J. Sound Vib. **43**, 9–20 (1975).
[14]K. M. Li, T. Waters-Fuller, and K. Attenborough, "Sound propagation from a point source over extended-reaction ground," J. Acoust. Soc. Am. **104**, 679–685 (1998).
[15]D. Takahashi, "Excess sound absorption due to periodically arranged absorptive materials," J. Acoust. Soc. Am. **86**, 2215–2222 (1989).
[16]A. R. Wenzel, "Propagation of waves along an impedance boundary," J. Acoust. Soc. Am. **55**, 956–963 (1974).
[17]S. Thomasson, "Reflection of waves from a point source by an impedance boundary," J. Acoust. Soc. Am. **59**, 780–785 (1976).
[18]C. Nocke, V. Mellert, T. Waters-Fuller, K. Attenborough, and K. M. Li, "Impedance deduction from broad-band, point source measurements at grazing incidence," Acust. Acta Acust. **83**, 1085–1090 (1997).
[19]C. Nocke, "Improved impedance deduction from measurements near grazing incidence," Acust. Acta Acust. **85**, 586–590 (1999).
[20]J. F. Allard, M. Henry, V. Gareton, G. Jansens, and W. Lauriks, "Impedance measurements around grazing incidence for nonlocally reacting thin porous layers," J. Acoust. Soc. Am. **113**, 1210–1215 (2003).
[21]G. Jansens, W. Lauriks, G. Vermeir, and J. F. Allard, "Free field measurements of the absorption coefficient for nonlocally reacting sound absorbing porous layers," J. Acoust. Soc. Am. **112**, 1327–1334 (2002).
[22]R. Lanoye, G. Vermeir, W. Lauriks, R. Kruse, and V. Mellert, "Measuring the free field acoustic impedance and absorption coefficient of sound absorbing materials with a combined particle velocity-pressure sensor," J. Acoust. Soc. Am. **119**, 2826–2831 (2006).
[23]F. V. Hunt, "Investigation of room acoustics by steady-state transmission measurements. I," J. Acoust. Soc. Am. **10**, 216–227 (1939).
[24]Y. W. Lam, "Issues for computer modelling of room acoustics in non-concert hall settings," Acoust. Sci. & Tech. **26**, 145–155 (2005) (available online from Acoustical Society of Japan).
[25]K. Sato and M. Koyasu, "Dependence of sound absorption coefficient upon area of acoustic materials," J. Acoust. Soc. Am. **31**, 628–629 (1959).
[26]E. D. Daniel, "On the dependence of absorption coefficients upon the area of the absorbent material," J. Acoust. Soc. Am. **35**, 571–573 (1963).
[27]T. Ten Wolde, "Measurement on the edge-effect in reverberation rooms," Acustica **18**, 207–212 (1967).
[28]A. Levitas and M. Lax, "Scattering and absorption by an acoustic strip," J. Acoust. Soc. Am. **23**, 316–322 (1951).
[29]R. K. Cook, "Absorption of sound by patches of absorbent materials," J. Acoust. Soc. Am. **29**, 324–329 (1957).
[30]T. D. Northwood, M. T. Grisaru, and M. A. Medcof, "Absorption of sound by a strip of absorptive material in a diffuse sound field," J. Acoust. Soc. Am. **31**, 595–599 (1959).
[31]A. De Bruijn, "A mathematical analysis concerning the edge effect of sound absorbing materials," Acustica **28**, 33–44 (1973).
[32]W. Lauriks, A. Cops, and Ph. Belien, "The influence of the edge effect on the statistical absorption coefficient," Acustica **70**, 155–159 (1990).
[33]M. Spivack, "Solution of the inverse scattering problem for grazing incidence upon a rough surface," J. Opt. Soc. Am. A **8**, 1892–1897 (1991).
[34]M. Spivack, "Coherent field and specular reflection at grazing incidence on a rough surface," J. Acoust. Soc. Am. **95**, 694–700 (1994).
[35]D. Habault, "Sound propagation above an inhomogeneous plane: Boundary integral equation methods," J. Sound Vib. **100**, 55–67 (1985).
[36]S. N. Chandler-Wilde and D. C. Hothersall, "Sound propagation above an inhomogeneous impedance plane," J. Sound Vib. **98**, 475–491 (1985).
[37]Y. Kawai and H. Meotoiwa, "Estimation of the area effect of sound absorbent surfaces by using a boundary integral equation," Acoust. Sci. & Tech. **26**, 123–127 (2005) (available online from Acoustical Society of Japan).
[38]P. M. Morse and K. U. Ingard, "The scattering of sound," in *Theoretical Acoustics* (McGraw-Hill, New York, 1968), Chap. 8, pp. 454–463.
[39]D. F. Mayers, "Quadrature methods for Fredholm equations of the second kind," in *Numerical Solutions of Integral Equations*, edited by L. M. Delves and J. Walsh (Oxford University Press, London, 1974), Chap. 6, pp. 64–79.
[40]M. C. Junger and D. Feit, "Elastic scatterers and waveguides," in *Sound, Structures, and Their Interaction* (Acoustical Society of America, New York, 1993), Chap. 11, pp. 342–387.